Journal of Ceramic Processing Research. Vol. 21, No. 3, pp. 343~350 (2020)
(Received 12 March 2020, Received in revised form 20 March 2020, Accepted 20 March 2020)
https://doi.org/10.36410/jcpr.2020.21.3.343

J O U R N A L O F
Ceramic Processing Research

Optimization of low temperature hydrogen sensor using nano ceramic-particles for use in hybrid electric vehicles

J. Niresh[a,*], N. Archana[b], S. Neelakrishnan[c], V. M. Sivakumar[d] and D. S. Dharun[e]
[a]*Assistant Professor, Department of Automobile Engineering, PSG College of Technology, Coimbatore, India*
[b]*Assistant Professor, Department of EEE, PSG College of Technology, Coimbatore, India*
[c]*Professor, Department of Automobile Engineering, PSG College of Technology, Coimbatore, India*
[d]*Associate Professor, Department of Chemical Engineering, Coimbatore Institute of Technology, Coimbatore, India*
[e]*PG Scholar, Department of Automobile Engineering, PSG College of Technology, Coimbatore, India*

Hydrogen sensing in automobile application is the need of the hour as fuel cell based hybrid electric vehicle is developing at a faster pace. Nickel ferrite ($NiFe_2O_4$) nanoparticles embedded reduced graphene oxide (rGO) prepared by a facile hydrothermal thermal process was employed as a chemiresistive sensor for the detection of H_2 gas. To study the morphological and structural features the synthesized samples were characterized by transmission electron microscopy (TEM), X-Ray diffraction and Raman Spectroscopy. 50 nm cube shaped $NiFe_2O_4$ nanoparticles were found to be distributed on few layered rGO nanosheets. The electrical conductivity of pristine n type $NiFe_2O_4$ and $NiFe_2O_4$/rGO were tested at various operating temperatures. Hydrogen sensing characteristics were measured by forming a thick film of the synthesized nanocomposite paste on an alumina substrate. Sensing results showed that $NiFe_2O_4$/ 1% rGO showed the maximum response at an optimum temperature of 80 °C towards 200 ppm of hydrogen gas among four variants. Integration of $NiFe_2O_4$ nanoparticles on rGO nanosheets has markedly enhanced the conductivity of the nanocomposite. The sensor showed a lower detection limit of 8 ppm with two linear ranges from 30-90 ppm and 100 to 700 ppm. Further the sensor was tested for its selectivity and stability.

Keywords: Hydrogen sensor, Nanoparticles, Chemiresistive, Electric Vehicles.

Introduction

With the growing population, the need for alternate green source of energy has become inevitable due to the depletion of fossil fuels. Among the various natural fuel sources, hydrogen is considered as the next generation energy source especially in the automobile industry [1, 2]. It has found its prominence due to extraordinary properties such as high energy content, no release of harmful gases on combustion and low molecular weight [3, 4]. Nevertheless, H_2 is highly volatile and flammable in nature. A small leak into the atmosphere could cause explosion. Since H_2 being an odourless and a colorless gas, it cannot be detected by human senses, perhaps special sensors are required. In order to safely exploit the benefits of H_2 energy, it is inevitable to develop sensors that can detect H_2 specifically from a mixture of gas. Among the various hydrogen sensors available such as electrochemical sensors, gasochromic sensors, fiber optic etc, chemiresistive sensors seem to be a good choice [5, 6]. Recently, it is known from the literature that carbon based materials can detect H_2 at room temperature and also they tend to shown high conductivity with the adsorption of H_2 on its network [7, 8]. Carbon nanomaterials such as graphene based gas sensors have attracted huge attention due to their stunning electrical and electronic properties [9-12]. Graphene has a high theoretical surface area (2630 m^2g^{-1}) and electrical conductivity (10^6 Scm^{-1}) which makes it a promising material for H_2 sensing [13]. A derivative of graphene which can be easily synthesized by chemical route is called reduced graphene oxide (rGO). Most graphene based gas sensors are increasingly being employed owing to three reasons [9]:

1. Its abundant defects and chemical groups facilitate gas adsorption
2. The chemical and electrical properties of rGO are highly tuneable by composite formation
3. Compared to its precursor Graphene oxide, rGO has high charge transfer rate.

Though numerous rGO based H_2 sensors have been developed, pristine graphene sensors suffer from low chemisorption of target gas molecules because of a few dangling bonds present on their surface. In a graphene stack, due to the van der Waals and π-π interactions among individual graphene there is high tendency for aggregation when its dispersion is dried. Integration of nanostructures with gas-sensing ability into graphene

*Corresponding author:
Tel : +91422 4344281
E-mail: nireshcbe@gmail.com

sheets inhibits agglomeration in graphene and also aids in good distribution of nanostructures. Thus, the effective surface area available for the gas interaction increases several fold [14].

To date, quite a few rGO based composite materials have been synthesized by incorporation of metal nanoparticles for better sensing properties [15-19]. However, the glitches with the traditional Pt, Pd nanoparticles is that they exhibit very high recovery time due to the formation of hybrids on hydrogen exposure. On the other hand, semiconducting metal oxides such as SnO_2, ZnO, CoO, TiO_2, Fe_2O_3 are also being used for gas sensing applications due to their easy implementation, good reliability and low cost in real time systems [20-22]. Gas sensing is a surface phenomenon where the adsorption of gases can alter the conductivity of the metal oxides. Depending on the operating temperature and the morphology of the metal oxide nanoparticles, distribution of various oxygen species such as O^-, O_2^- and O_2^- differs [23]. Han et al fabricated functionalized RGO that demonstrates excellent sensitivity to H2S gas. The functionalization process used GO suspensions mixed with $AgNO_3$, NaOH, and DI water [24]. Shivi et al. studied the Surface Enhanced Raman Spectroscopy of reduced graphene oxide modified with silver nanoparticles. They found that the D peak, G peak and 2D peak intensity of Raman spectra has been amplified many times with silver nanoparticles as well as silver nanoparticles intercalate between the layers of graphene oxide, therefore it is also helpful in reduction of graphene oxide [25].

Although metal oxide nanoparticles increase the sensitivity, the selectivity is dependent on dopants. However from literature it has been understood that controlling the shape of the nanocrystallites can effectively change energy of different adsorption sites thereby adsorbing gases at a lower temperature. Thus, the existence of large surface to volume ratio in metal oxides yield better performance [26]. Nevertheless, metal oxides as individual sensing units detect hydrogen only at elevated temperatures due to wide band gap and high electrical resistance in the range of kilo to mega ohms.

Multi component systems such as spinel nanostructures with general formula of AB_2O_4 are noteworthy materials to detect both oxidizing and reducing gases. Among the spinel type structures, ceramic $NiFe_2O_4$ finds its application in sensing gases like Cl_2, NH_3 etc, dye degradation, Li-ion batteries and magnetic hyperthermiac [27-32]. It exhibits excellent stability, electrochemical activity and electrical conductivity that arises due to thermal activation of electrons or holes in the ionic lattice. Usually, the charge transfer occurs through hopping process between the cations of different valences at a low activation energy. The oxygen atom of $NiFe_2O_4$ occupies the FCC position and the cations Fe^{3+} and Ni^{2+} occupy the tetrahedral and octahedral positions. During the synthesis of $NiFe_2O_4$ by hydrothermal process, Fe^{2+} ions always forms with Fe^{3+}. In order to compensate the charge imbalance, positive oxygen vacancies are created. The electrons hop between the cations of different valences in O^- sites providing the necessary active metal centres for adsorption of analyte gas molecules thereby facilitating the catalytic activity [32]. When these spinel nanostructures are supported on graphene carbon network, they are known to exhibit improved stability as well as electrochemical response. For instance, compared to pristine $NiFe_2O_4$, $NiFe_2O_4$/rGO showed higher HER activity [33]. Liu et al. reported that mixing of $ZnFe_2O_4$ into graphene can lower the operating temperature of acetone sensors [34]. Lin et al showed that graphene/CuO composites can detect low level of NO_2 at room temperature [35]. The performance improvement of these nanocomposites are attributed to the presence of multiple redox states which aid in the enhanced catalytic activity. Also, the synergistic effect between graphene and spinels adds novel properties to the hybrid. The detection of H_2 gas employing $NiFe_2O_4$ and rGO have not be reported till date. Herein, we report a facile synthesis of $NiFe_2O_4$/rGO by in-situ hydrothermal method. The synthesized material was used for the fabrication of a chemiresistive H_2 sensor with an improvement in response, recovery time and reduction in operating temperature.

Experimental Setup

Reagents

Graphite powder (Alfa Aesar), NaOH (HiMedia), $NaNO_3$ (HiMedia), H_2SO_4 (Merck), potassium permanganate ($KMnO_4$) (Merck), H_2O_2 (Merck), and chemicals such as HCl, $NiCl_2$ and $FeCl_3$ were purchased from Loba-Chemie. All the solutions were dissolved in dissolved water and used for the studies

Preparation of graphene oxide

Graphene oxide was synthesized by the modified Hummer's method, a well-established protocol to mass produce graphene oxide [36]. In short, 1.25 g of graphite powder was added to a precooled mixture of 25 mL H_2SO_4 and 1.25 g $NaNO_3$. To it, 3.75 g of $KMnO_4$, the oxidizing agent is added slowly under vigorous stirring. After addition the solution is stirred for 2 h at 35 ºC. Then 50 mL of water was added to the solution and the temperature was raised to 95 ºC and maintained for 15 min. Subsequently the solution was quenched with water and brought to room temperature. 10 mL of 30% H_2O_2 was added slowly and the solution was stirred for 10 min. The resulting solution was washed with 5% HCl to remove the metal ions and further with distilled water to raise the pH to 7. Lastly, washed solution was dried in an hot air oven at 90 ºC for 8 h to get powders of graphite oxide. To obtain graphene oxide, the graphite oxide powders were dissolved in water and ultrasonicated for 30 min.

Preparation of $NiFe_2O_4$/rGO

0.1 M $NiCl_2$ and 0.2 M of $FeCl_3$ were mixed in 50 mL distilled water. To it 0.01 M of NaOH and different concentration of GO (0.5%, 1%, 1.5% and 2%) was added and the solution was stirred well in a magnetic stirrer at 300 rpm for 10 min. The mixture was then transferred to a teflon lined autoclave and heated at 180 ºC for 12 h. The resting solution was centrifuged, washed with water and dried under vacuum. The powders were then subjected to calcination at 400 ºC.

Material characterisation

The morphology of the nanocomposite was studied using Transmission electron microscope (TEM) from JEOL JEM 2100. The X-ray diffraction (XRD) pattern was recorded from Bruker DS Advance with Cu Kα as radiation source with a wavelength of 1.54 Å. The Laser Raman spectroscopy was done using Renishaw inVia fitted with 785 nm laser.

To fabricate the sensor, a thick film of the composite paste was made on a clean alumina substrate having copper electrical contacts. The paste was prepared by mixing sufficient amount of ethanol to the synthesized powder. A film of 50 μm thickness was coated on the substrate. The fabricated sensor was then placed in a test chamber at appropriate temperature and other environmental conditions. As a known quantity of H_2 gas is passed, change in voltage with across a resistor connected in series with the fabricated resistor was recorded using a Keithley data acquisition module KUSB-3100 interfaced with a computer. The sensor performance is given as Ra/Rg ratio where Ra and Rg are the resistances in the presence of air and saturated H_2 gas respectively. The time taken by the sensor to reach 90% of the total resistance change in case of adsorption is determined as response time and in case of desorption the time taken for the sensor to reach 10% of the total resistance is determined as recovery time. All the fabricated sensors were tested following the above procedure at varying temperatures of 20 to 200 ºC with an interval of 20 ºC.

Results and Discussion

Material characterisation

The $NiFe_2O_4$/rGO based H_2 sensor was constructed

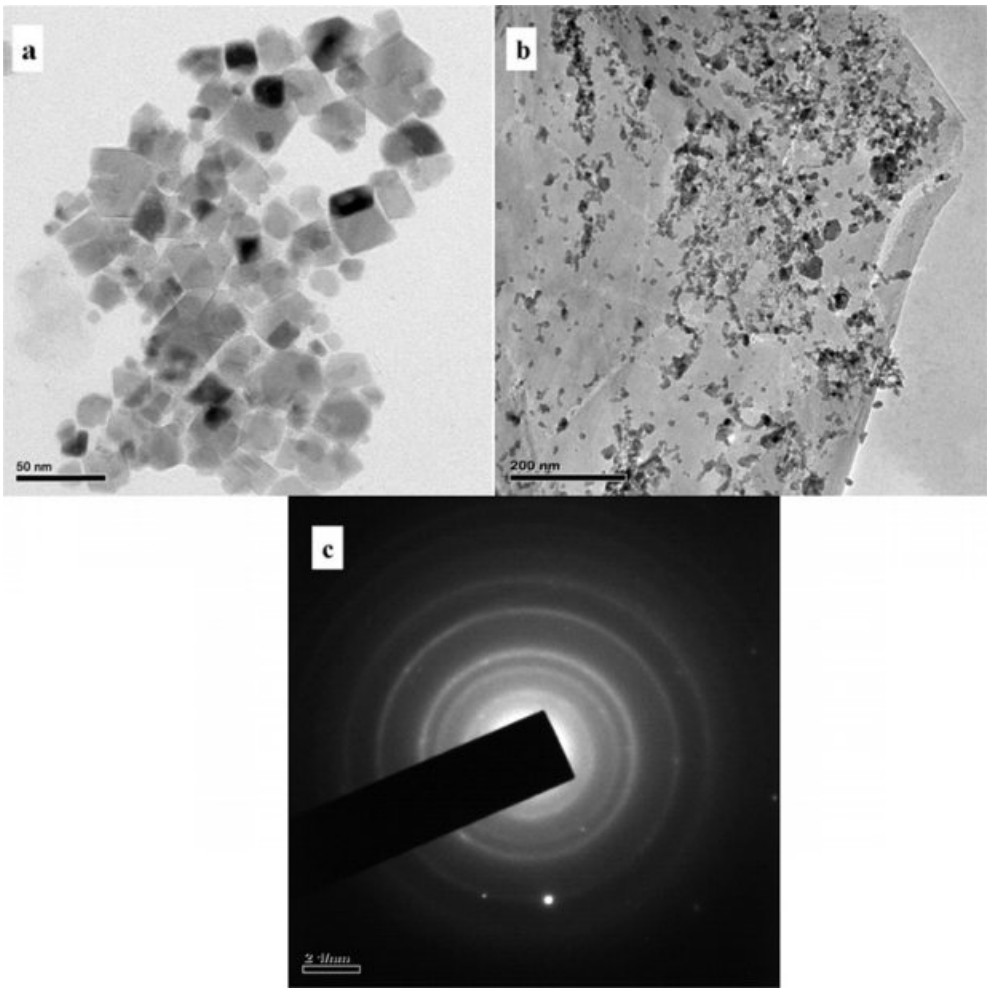

Fig. 1. TEM images of (a) $NiFe_2O_4$ (b) $NiFe_2O_4$/1% rGO and (c) SAED pattern of $NiFe_2O_4$/1 % rGO.

based on the electrostatic interaction between the moieties. The oxygen functional groups present in the graphene oxide increases the hydrophilicity of the material. The $NiFe_2O_4$ were prepared by the in-situ co-precipitation of $NiCl_2$ and $FeCl_3$ in the presence of GO at elevated temperatures. During the process, GO loses most of its functional groups and $NiFe_2O_4$ are anchored on the rGO matrix through an electrostatic interaction between the spare functional groups of rGO and $NiFe_2O_4$ nanoparticles. Fig. 1 shows the TEM images of $NiFe_2O_4$ and $NiFe_2O_4$/rGO respectively. $NiFe_2O_4$ produced by co-deposition showed a cube like morphology with an average particle size of 55 nm. Fig. 1(b) clearly depicts a good distribution of $NiFe_2O_4$nanoparticles anchored on sheets like structure of rGO. Also rGO was found to be transparent with few layers and high surface area. Fig. 1(c) shows the SAED pattern of the composite.

Fig. 2 depicts the XRD pattern of pristine $NiFe_2O_4$ and $NiFe_2O_4$/rGO composite. The sharp peaks indicate the crystalline nature of the nanocomposite. Both the materials exhibit sharp peaks which could be indexed to (220), (311), (222), (400), (422), (511) and (440) planes of the cubic and face centered structure of $NiFe_2O_4$. The values were in accordance with the JCPDS number 54-0964.

Fig. 3 shows the Raman spectrum of GO and $NiFe_2O_4$/1% RGO. Two prominent peaks at 1,339 cm^{-1} and 1,589 cm^{-1} were observed in the Raman spectrum of GO corresponding to D and G band respectively. The G band corresponds to the E_{2g} mode linked to sp2 carbon vibrations and D band corresponds to that of sp3 carbon atoms of defects and disorders. In addition to D and G band few other bands with lower intensity in the spectral range of 500-700 cm^{-1} were observed for $NiFe_2O_4$/rGO which are characteristic bands for the spinel type $NiFe_2O_4$. The I_D/I_G value of the rGO composite was higher (1.1) compared to GO (0.99) which indicates the presence of sp3 defects upon reduction or interaction with $NiFe_2O_4$.

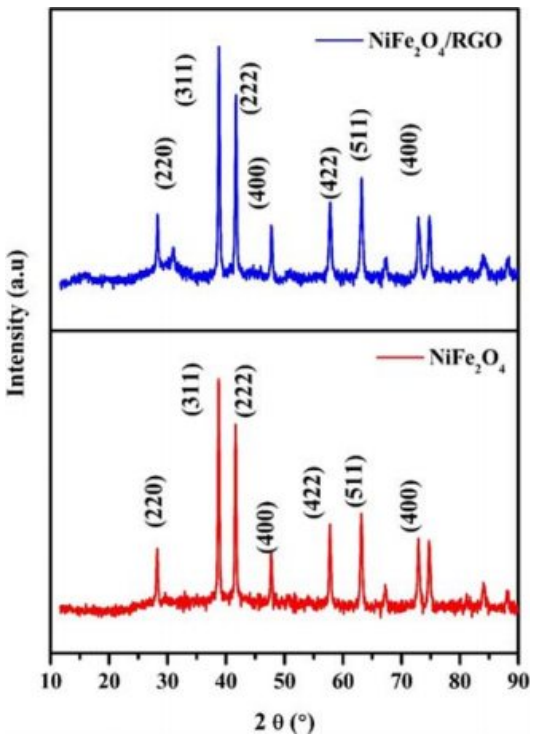

Fig. 2. XRD pattern of $NiFe_2O_4$ and $NiFe_2O_4$/1% rGO.

Electrical characterisation

The resistance of $NiFe_2O_4$ and $NiFe_2O_4$/rGO with the raise in temperature is measured and is shown in Fig. 4. Since $NiFe_2O_4$ being n type in nature exhibited a reduction in resistance with an increase in temperature. Also due to the combination of $NiFe_2O_4$ with a highly conductive rGO sheets, a relatively higher resistance decrease is observed. Similar improvement in conductivity of metal oxides WO_3 and ZnO anchored on rGO sheets were observed by Qin et al and Anand et al.

H_2 sensing Characteristics

To determine the optimum temperature for H_2 sensing, temperature studies were performed from 40 ºC to 200 ºC in steps of 20 ºC and at each temperature a constant H_2 concentration of 200 ppm was maintained. Fig. 5 shows the sensor response vs. operating temperature of pristine $NiFe_2O_4$ and $NiFe_2O_4$/rGO nanocomposite at various additions of rGO. From the Fig it can be clearly observed that with the increase in temperature the conductivity increases. All the rGO composites showed the maximum sensor performance at an optimum operation temperature of 80 ºC. On the other hand, $NiFe_2O_4$ showed relatively lower performance at an operating temperature of 140 ºC. With addition of rGO, there is a clear improvement in the sensing performance. The enhanced performance is attributed to the incorporation of $NiFe_2O_4$ into rGO which increases the effective

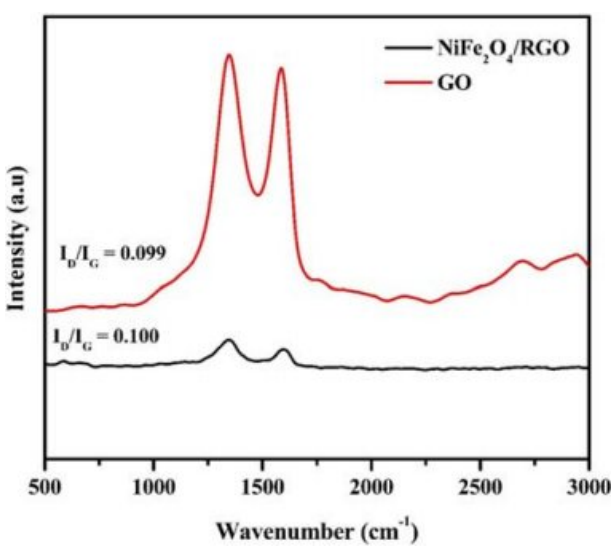

Fig. 3. Raman spectrum of $NiFe_2O_4$ and $NiFe_2O_4$/1% rGO.

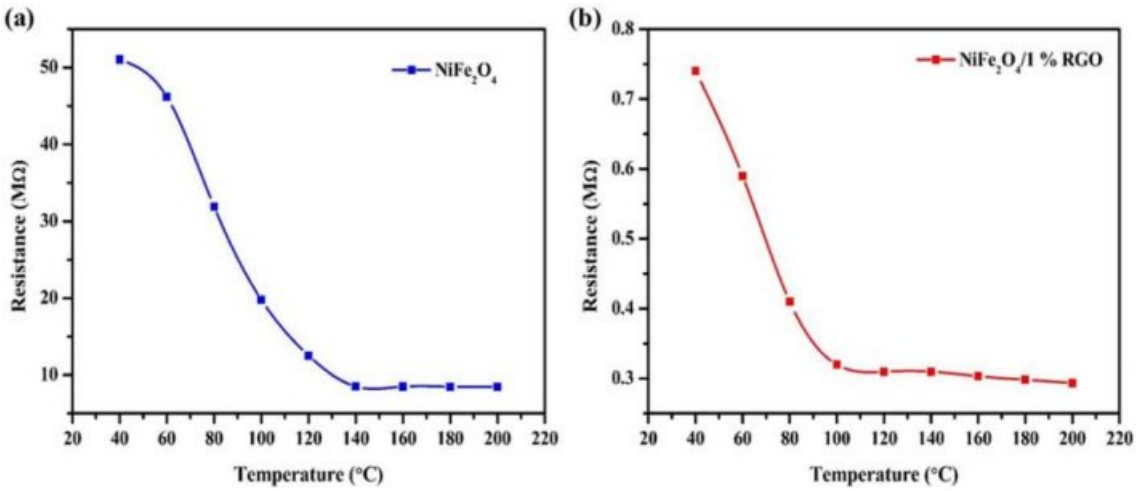

Fig. 4. Resistance Vs. temperature response curves of (a) $NiFe_2O_4$ and (b) $NiFe_2O_4$/1% rGO.

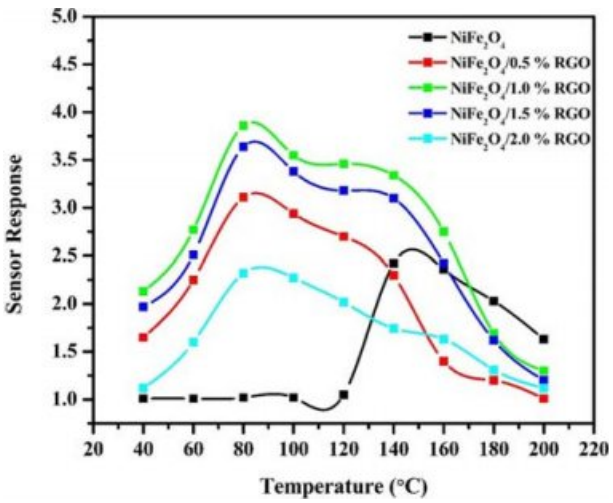

Fig. 5. Sensing response vs. operating temperature of $NiFe_2O_4$ and $NiFe_2O_4$/rGO for a H_2 concentration of 200 ppm.

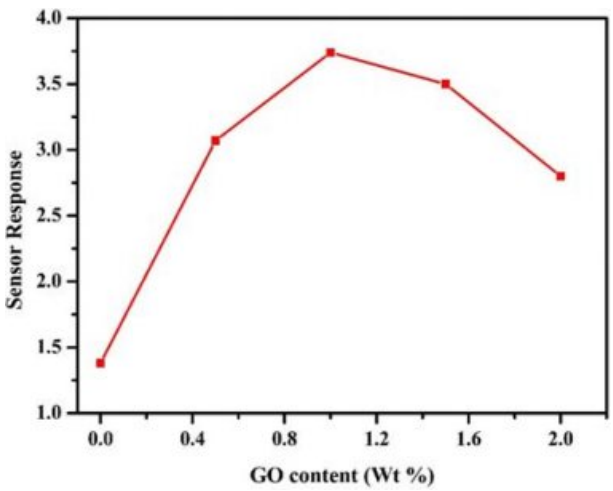

Fig. 6. Sensor response towards 200 ppm of H_2 for different GO content in $NiFe_2O_4$/rGO composite at an optimum temperature of 80 °C.

active surface area of gas interaction. Also, it can be seen that $NiFe_2O_4$/1% rGO marked the highest performance among all the different compositions and hence was chosen for subsequent sensing characterization. With increase in rGO concentration above 1%, there is a possibility of agglomeration which could lead to decreased active surface area and hence low performance.

To determine the response and recovery time, pristine $NiFe_2O_4$ and $NiFe_2O_4$/1% rGO was subjected to 200 ppm of H_2 at their operating temperature. Fig. 6 shows that the composite showed quicker response of 28 s and recovery time of 85 s. To further comprehend the effect of temperature on sensor performance, the response time and recovery time were measured at various operating temperatures for $NiFe_2O_4$/1 % rGO composite and the results are given in Table 1. From the table it can be visualized that with the increase in temperature there is a reduction in both response and recovery time. Also at temperature beyond 80 ºC there is no significant change in the response and recovery times. In fact with higher temperature the peak response value degraded as observed in Fig. 5.

Table 1. $NiFe_2O_4$/1% rGO sensor response and reaction kinetics vs operating temperature

Parameters	Temperature (ºC)		
	40	60	80
Response (R_a/R_g)	2.1	2.80	3.85
Response time (s)	92	58	32
Recovery time (s)	144	118	85

Detection of H_2 gas

The $NiFe_2O_4$/1% rGO composite sensor performance towards different concentration of H_2 is depicted in Fig. 7. At higher concentration from 100 ppm to 700 ppm, a linear response trend was observed. Beyond 800 ppm there was no significant rise in the response due to the

saturation of the active adsorption sites. At lower concentrations from 10 ppm to 100 ppm, there was no linearity, however there was a steep linear response after a concentration of 30 ppm. Such kind of response is due to the fact that at lower concentrations, the gas molecules adsorbed to the active sites form a monolayer. With an increasing concentration, subsequent layers are formed thereby the response is dominated by the multilayer adsorption. The sensor showed a limit of detection (LOD) of 8 ppm. LOD is the lowest concentration of gas detected by the sensor. The detection limit was determined by supplying known volume of gas into the test chamber and measuring the change in resistance as shown in Table 1. The resistance given by $NiFe_2O_4$/1% rGO in air is 0.185×10^6 Ω. A significant change in the resistance for a particular gas concentration was regarded as the lowest detection limit of the sensor. The H_2 sensor characteristics exhibited by $NiFe_2O_4$/rGO is compared with other metal oxides and is shown in Table 2.

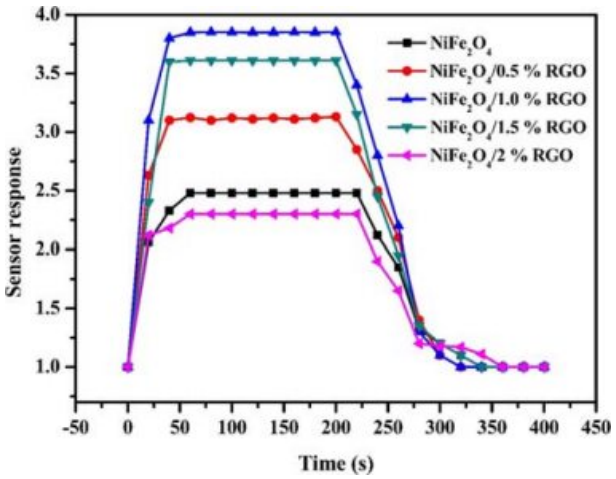

Fig. 7. Sensor response vs. time graph of $NiFe_2O_4$ and $NiFe_2O_4$/rGO composite for a H_2 concentration of 200 ppm at their respective operating temperature.

Table 2. Resistance values of $NiFe_2O_4$/1% rGO for H_2 concentration from 2 ppm-10 ppm

S.No	Concentration of H_2 (ppm)	Resistance, R_g (MΩ)
1	2	0.185
2	4	0.185
3	6	0.185
4	8	0.171
5	10	0.154

Interference studies

To determine the selectivity of the sensor, it was exposed to gases such as ammonia, H_2S_2, ethanol and LPG at 80 ºC. Fig. 7 shows the interference plot for 200 ppm of H_2 and equal volumes of the other gases. Only around 10% response was exhibited by the sensor for ammonia, H_2S_2 and ethanol showing a remarkable selectivity for H_2. However there was a 20% response for LPG leading to small but significant interference.

Stability studies

The stability of the sensor was determined by maintaining a concentration of 200 ppm and measuring the resistance continuously for 1 h by continuous hydrogenation and dehydrogenation for every 6 min (Results not shown). Almost 93% of the response was retained after 6 cycles which shows the excellent reproducibility and stability of the sensor.

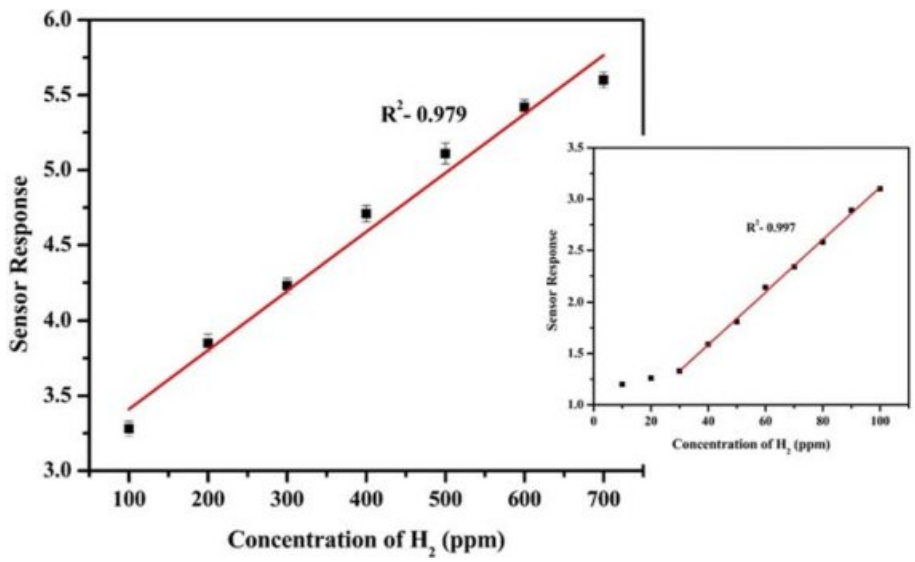

Fig. 8. Sensing response of $NiFe_2O_4$/1% rGO at operating temperature for H_2 concentration from 100 to 700 ppm and inset shows sensor response for 10-100 rpm.

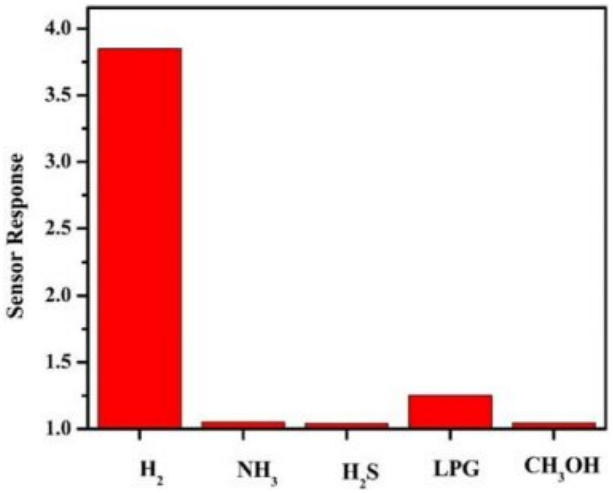

Fig. 9. Interference plot of $NiFe_2O_4$/1% rGO showing sensor response for 200 ppm of different gases at an operating temperature of 80 °C.

Conclusion

$NiFe_2O_4$/rGO were prepared by a facile hydrothermal method and employed as a chemiresistive H_2 sensor. The synthesized materials were characterized by TEM, XRD and Raman spectroscopy which showed the morphology and structural pattern of the composite. The electrical characterization showed the n type behavior of both pristine $NiFe_2O_4$ and $NiFe_2O_4$/rGO thereby with the adsorption of gas increase in conductivity is expected to occur. The gas sensing characteristics of the composite were studied at different operating temperature with four variants. The nanocomposite with 1 wt % rGO showed a higher response to H_2 sensing at an operating temperature of 80 ºC. Also a very low response and recovery time of 32 s and 85 s were observed. Further the sensor showed good sensitivity, selectivity and stability in the presence of interfering gases. It is concluded that with the incorporation of rGO there is an increased electron transfer facilitating a decrease in resistance and thereby better performance.

References

1. T. Hübert, L. Boon-Brett, G. Black, and U. Banach, Sensor Actuat. B Chem. 157 (2011) 329-352.
2. V. Tozzini, and V. Pellegrini, Phys. Chem. Chem. Phys. 15 (2013) 80-89.
3. P. Jena, J. Phys. Chem. Lett. 2 (2011) 206-211.
4. L. Schlapbach, and A. Züttel, in Materials for sustainable energy a collection of peer-reviewed research and review articles from nature publishing group. (2011) 265-270.
5. L. Boon-Brett, J.Bousek, and P.Moretto, Int. J. Hydrog. Energy 34 (2009) 562-571.
6. F. Favier, E.C. Walter, M.P. Zach, and T. Benter, and R.M. Penner, Science 2001293 (5538) 2227-2231.
7. S. Dhall, K. Sood, and R. Nathawat, Int. J. Hydrog. Energy 42 (2017) 8392-8398.
8. A. Kaniyoor and S. Ramaprabhu, Carbon 49 (2011) 227-236.
9. F.L. Meng, Z. Guo, and X.J. Huang TRAC-Trends Anal. Chem. 68 (2015) 37-47.
10. N. Joshi, T. Hayasaka, Y. Liu, H. Liu, O.N. Oliveira, and L. Lin Microchim.Acta 185 (2018) 213.
11. T. Wang, D. Huang, Z. Yang, S. Xu, G. He, X. Li, N. Hu, G. Yin, D. He, and L. Zhang, Nano-Micro Lett. 8 (2016) 95-119.
12. F.L. Meng, Z. Guo, and X.J. Huang TRAC-Trends Anal. Chem. 68 (2015) 37-47.
13. K.S. Novoselov, A.K. Geim, S.V. Morozov, D. Jiang, Y. Zhang, S.V. Dubonos, I.V. Grigorieva, and A. Firsov, Science 306 (2004) 666-669.
14. S.S. Varghese, S. Lonkar, K.K. Singh, S. Swaminathan, and A. Abdala, Sensor Actuat. B Chem. 218 (2015) 160-183.
15. N. Joshi, T. Hayasaka, Y. Liu, H. Liu, O.N. Oliveira, and L. Lin, Mikrochim.Acta 185 (2018) 213.
16. A. Pandey, N.R. Wilson, and J.A. Covington, Sensor Actuat. B Chem. 183 (2013) 478-487.
17. M.G. Chung, D.H. Kim, D.K. Seo, T. Kim, H.U. Im, H.M. Lee, J.B. Yoo, S.H. Hong, T.J. Kang, and Y.H. Kim, Sensor Actuat. B Chem. 169 (2012) 387-392
18. B. Alfano, T. Polichetti, M.L. Miglietta, E. Massera, C. Schiattarella, F. Ricciardella, and G. Di Francia, Sensor Actuat. B Chem. 239 (2017) 1144-1152.
19. D. Gupta, D. Dutta, M. Kumar, B. Barman, C.K. Sarkar, S. Basu, and S.K. Hazra, Sensor Actuat. B Chem. 196 (2014) 215-222.
20. J.X. Wang, X.W. Sun, Y. Yang, H. Huang, Y. Lee. O.K. CTan, and L. Vayssieres, Nanotechnology 17 (2006) 4995.
21. W. Wu, M Zeng, and Y. Li, Mater.Lett. 104 (2013) 34-36.
22. M.A Kozhushner, L.I. Trakhtenberg, A.C. Landerville, and I.I. Oleynik, J. Phys. Chem. C 117 (2013) 11562-11568.
23. S.L. Darshane, S.S. Suryavanshi, and I.S. Mulla, Ceram. Int. 35 (2009) 1793-1797.
24. H.G. Na, Y.J. Kwon, S.Y. Kang, W. Kang, M.S. Choi, J.H. Bang, T.K. Jung, C. Lee, and H.W. Kim, J Ceramic Processing Research 17[6] (2016) 523-531.
25. S. Rathore, D.K. Patel, and P.-D. Hong, J Ceramic Processing Research 20[4] (2019) 442-448.
26. G. Korotcenkov, Sens. Actuators B 107 (2005) 209-232.
27. R. Hajihashemi, A.M. Rashidi, M. Alaie, R. Mohammadzadeh, and N. Izadi, Mater. Sci. Eng. C 44 (2014) 417-421.
28. J.Y. Patil, D.Y. Nadargi, J.L. Gurav, I.S. Mulla, and S.S. Suryavanshi, Mater. Lett. 124 (2014) 144-147.
29. R.B. Kamble and V.L. Mathe, Sensor Actuat. B Chem. 131 (2008) 205-209.
30. Y. Fu, Y. Wan, H. Xia, and X. Wang, J. Power Sources 213 (2012) 338-342.
31. Y. Xiong Fu, L. Wang, and X. Wang, Chem. Eng. 195 (2012) 149-157.
32. W. Zhang, M.B. Jungfleisch, W. Jiang, J.E. Pearson, and A. Hoffmann, J. Appl. Phys. 117 (2015) 17C727.
33. A. Mukherjee, S. Chakrabarty, W.N. Su, and S. Basu, Mater.Today Energy 8 (2018) 118-124.
34. F. Liu, X. Chu, Y. Dong, W. Zhang, W. Sun, and L. Shen, Sensor Actuat. B Chem. 188 (2013) 469-474.
35. Q. Lin, Y. Li, and M. Yang, Sens. Actuators B 173 (2012) 139-147.
36. W.S. Hummers, R.E. Offeman, J. Am. Chem. Soc. 80 (1958) 1339.
37. J. Qin, M. Cao, N. Li, and C. Hu, J. Mater. Chem. 21 (2011) 17167-17174.

38. K. Anand, O. Singh, M. Singh, J. Kaur, and R.C. Singh, Sensor Actuat. B Chem. 195 (2014) 409-415.
39. A. Russo, N. Donato, S.G. Leonardi, S. Baek, D.E. Conte, G. Neri, and N. Pinna Angew. Chem. Int. Ed. 51 (2012) 11053-11057.
40. A. Venkatesan, S. Rathi, I.Y. Lee, J. Park, D. Lim, G.H. Kim, and E.S. Kannan, Semicond. Sci. Technol. 31 (2016) 125014.
41. A. Pandey, N.R. Wilson, and J.A. Covington, Sensor Actuat. B Chem. 183 (2013) 478-487.
42. F. Bayata, B. Saruhan-Brings, and M. Ürgen, Sensor Actuat. B Chem. 204 (2014) 109-118.
43. A. Katoch, Z.U. Abideen, H.W. Kim, and S.S. Kim, ACS Appl. Mater & Interfaces 8 (2016) 2486-2494.
44. C. Xiang, Z. She, Y. Zou, J. Cheng, H. Chu, S. Qiu, H. Zhang, L. Sun, and F. Xu, Ceram. Int. 40 (2014) 16343-16348.
45. L. Huo, X. Yang, Z. Liu, X. Tian, T. Qi, X. Wang, K. Yu, J. Sun, and M. Fan, Sensor Actuat. B Chem. 244 (2017) 694-700.
46. K. Nguyen, C.M. Hung, T.M. Ngoc, D.T.T. Le, D.H. Nguyen, D.N. Van, and H.N. Van, Sensor Actuat. B Chem. 253 (2017) 156-163.